Spatial sequestration of misfolded proteins by a dynamic chaperone pathway enhances cellular fitness to stress

Stéphanie Escusa-Toret, **Willianne I. M. Vonk**, and **Judith Frydman**

Department of Biology, Stanford University, Stanford, CA 94305, USA

Abstract

The extensive links between proteotoxic stress, protein aggregation and pathologies ranging from aging to neurodegeneration underscore the importance of understanding how cells manage protein misfolding. Using live-cell imaging, we here determine the fate of stress-induced misfolded proteins from their initial appearance until their elimination. Upon denaturation, misfolded proteins are sequestered from the bulk cytoplasm into dynamic ER-associated puncta that move and coalesce into larger structures in an energy-dependent but cytoskeleton-independent manner. These puncta, which we name Q-bodies, concentrate different misfolded and stress-denatured proteins en-route to degradation, but do not contain amyloid aggregates, which localize instead to the IPOD. Q-body formation and clearance depends on an intact cortical ER and a complex chaperone network that is affected by rapamycin and impaired during chronological aging. Importantly, Q-body formation enhances cellular fitness during stress. We conclude that spatial sequestration of misfolded proteins in Q-bodies is an early quality control strategy occurring synchronously with degradation to clear the cytoplasm from potentially toxic species.

Introduction

Misfolded proteins challenge the integrity of the cellular proteome and compromise cell viability[1] and compromise cell viability[2]. Their accumulation in insoluble protein aggregates is linked to neurodegenerative amyloid disorders, including Alzheimer's and Huntington's Disease[3]. Accordingly, cells evolved elaborating Quality Control (QC) machineries that eliminate misfolded proteins and maintain protein homeostasis[4, 5]. Molecular chaperones are central to this process, as they recognize non-native conformations and triage polypeptides for either refolding or degradation through the ubiquitin-proteasome pathway (UPS) or autophagy[4, 5]. In addition, cells can actively sequester misfolded proteins in defined QC compartments[6-8]. Upon proteasome impairment, misfolded proteins partition into spatially and functionally distinct compartments[6, 7]: the JUNQ (juxtanuclear quality-control compartment), which sequesters misfolded polypeptides in a detergent soluble state; and the IPOD (insoluble protein deposit), which sequesters terminally aggregated polypeptides[9, 10]. Amyloid proteins, such as poly Q-expanded Huntingtin, are partitioned primarily to the

Corresponding author: jfrydman@stanford.edu.

IPOD, even in the absence of proteasome inhibition[5]. Protein sequestration into these inclusions is proposed as an alternative cellular defense when QC machineries fail[11-13].

QC is currently viewed as a two-tiered system, whereby misfolded proteins are first either refolded or degraded through the action of chaperones and the UPS, and then, when triage fails, transported in a cytoskeleton-dependent manner to cellular QC inclusions[14]. By following, in real time, QC substrates in the absence of proteasome inhibition, we find instead that misfolded proteins are rapidly concentrated in many dynamic inclusions, which we term Q-bodies, even as they are degraded by the proteasome. Q-body formation and movement is independent of the cytoskeleton, but requires the cortical endoplasmic reticulum (ER) and the concerted action of a chaperone network. We propose that sequestration of misfolded proteins is an integral and early aspect of cellular QC that does not necessarily ensue from proteostasis impairment or cellular dysfunction. Our data have implications for understanding the genesis of terminal protein inclusions characterizing a wide number of human pathologies[1].

Results

Sequestration of misfolded proteins into dynamic puncta is an early quality control response

To understand QC in unperturbed yeast cells, we used live-cell microscopy to follow the fate of a thermolabile allele of *UBC9* (Ubc9-2 herein Ubc9ts) that is folded at 28°C (Ubc9ts-N; Fig. 1a) but denatures above 33°C (Ubc9ts-Den; Fig. 1a, b and Fig. S1a)[6]. Ubc9ts-GFP expressed from a galactose-inducible promoter at 28°C generated folded Ubc9ts (Ubc9ts-N), localized diffusely throughout the cell. We shut-off Ubc9ts expression by addition of glucose and shifted the cells to 37°C, causing the pre-existing Ubc9ts to misfold and be degraded with a half-life of approximately 15-20 min (Fig. 1c and d). The UPS is the major degradation pathway for misfolded Ubc9ts since inhibition of autophagy by deletion of Atg8[15] produced only a minor stabilization of Ubc9ts (Fig. 1e and Fig. S1b). As reported[6], proteasome inhibition leads to Ubc9ts accumulation into the JUNQ and IPOD (Fig. 1c).

The dynamics and fate of misfolded Ubc9ts-GFP during the process of degradation was visualized in live cells by epifluorescence microscopy following expression shut-off (Fig. 1f, video S1). Shortly after shifting to 37°C, an increasing number of dim scattered Ubc9ts-GFP puncta appeared throughout the cytosol. Within 5 minutes, 5 to 10 puncta were clearly observed in the medial focal plane (Fig. 1f). Between 5 and 30 minutes, the diffuse signal disappeared as the dim Ubc9ts-GFP puncta coalesced into fewer and brighter structures that continued to merge even as Ubc9ts was cleared from the cell (Fig. 1f, g and video S1). Wild-type Ubc9-GFP remained diffuse and soluble at 37°C and did not form puncta (Fig. S1c), confirming these inclusions arise from Ubc9ts misfolding. Quantification of the average number of puncta in a medial focal plane at 5 min intervals during a 60 min movie indicated a consistent decrease in puncta number from 5 to 30 min (Fig. 1h). All puncta disappeared within an hour. Similar results were obtained when Ubc9ts was misfolded at 33°C, indicating that this pathway is not specific to higher temperature stress (Fig. S1a). Upon proteasome inhibition, the formation and early coalescence of Ubc9ts-GFP puncta occur similarly to untreated cells, albeit with a slightly higher number of puncta (Fig. 1h),

which continue coalescing into 1-3 large inclusions[6] (Fig. 1c, d). These results suggest that the JUNQ, the IPOD, and other inclusions observed upon proteasome inhibition[7] may result from the accumulation of coalesced puncta over time as their clearance is impaired.

We conclude that misfolded proteins do not remain diffusely distributed in the cytosol, but are also not deposited into a static pre-existing compartment. Instead, they are collected and processed through a dynamic cellular pathway into multiple punctate structures throughout the cell which by coalescence, mature into larger inclusions. By analogy to the dynamic P-body-mediated RNA QC[16], we propose to name these protein QC structures Q-bodies.

Q-body dynamics are energy dependent but cytoskeleton independent

Tracking the trajectory of Q-bodies *in vivo* did not reveal any directional movement suggesting they do not move on defined tracks (Fig. 1i). The average speed of puncta was 5 to 15 nm/s, i.e. about 10 times slower than endocytic particles moving on the cytoskeleton[17] and did not change appreciably before (black trace) and after (gray trace) coalescence with another puncta (Fig. 1i). This led us to examine the role of the cytoskeleton on Q-body dynamics. The actin and microtubule cytoskeletons were disrupted with 200 μM of latrunculin A (LatA) and 15 μm/mL nocodazole (Noc), respectively, followed by imaging of Ubc9ts-GFP (Fig. 2a, b and c top panels). A 10 min LatA treatment prior to induction of Ubc9ts misfolding completely disrupted the actin cytoskeleton, as confirmed by imaging the actin binding protein Abp1-GFP (Fig. 2a). Nonetheless, Q-bodies were still formed, processed and degraded similar to WT (Fig. 2a, video S2). Tracking analysis indicated that LatA treatment did not measurably affect the average speed or directionality of Q-bodies over their lifetime (Fig. 2a, lower panel). Of note, prolonged incubation (2 hours) with LatA did perturb Q-body formation and movement (Fig. 2b) suggesting that prolonged disruption of the actin cytoskeleton impairs protein homeostasis. The tubulin cytoskeleton is also dispensable for Q-body formation and dynamics. 10 min treatment with Noc disrupted microtubules, but did not affect Q-body dynamics and clearance (Fig. 2c). We conclude that neither Q-body formation nor dynamics requires a functional actin and tubulin cytoskeleton.

We next assessed whether Q-body formation and movement require energy. Intracellular ATP depletion with sodium azide and deoxyglucose for 30 min (Fig. 2d) did not abrogate Q-body formation, suggesting that this step is energy independent. However, Q-body dynamics, coalescence and clearance were highly perturbed (Fig. 2d, video S3). We conclude that that the concentration of misfolded protein into Q-bodies is energy independent, whereas their movement, coalescence and clearance require ATP.

Q-body formation and processing requires an intact cortical ER

We next sought to identify cellular structures associated with Q-bodies. Because the JUNQ colocalizes with the perinuclear ER[6], Ubc9ts was co-expressed with the nuclear marker Npl3, or with perinuclear ER protein Hmg1 (Fig. 3a and b)[18]. Z-sections of deconvolved images revealed the distribution of Ubc9ts Q-bodies vis-à-vis the nucleus (Fig. 3a and b). In each cell analyzed, at least one puncta was juxtanuclear, while the others were distributed throughout the cell.

No obvious colocalization of Q-bodies was observed with early endosomes (GFP-Snc1), late endosomes (GFP-Pep12), vacuole (MDY64), autophagic structures (CHFP-Atg8) and the spindle pole body (Spc42-GFP) (Fig. S2a, b). Given the vicinity of one inclusion with the perinuclear ER, we examined Q-body association with the cortical ER, extending as a tubular network throughout the cell[19]. Two-color Z-stacks of deconvolved images from cells expressing Ubc9ts-CHFP and the cortical ER marker Rtn1-GFP revealed a close proximity between Q-bodies and cortical ER tubules (Fig 3c, d, and video S4).

The role of the cortical ER in Q-body dynamics was assessed in *rtn1 rtn2 yop1* cells, whose cortical ER morphology is disrupted[20-22]. A large Ubc9ts inclusion was already observed at the permissive temperature (Fig. 3e). At 37°C, a few additional dim puncta appeared and coalesced with the large inclusion (Fig. 3e, video S5). After 30 minutes at 37°C, when most misfolded Ubc9ts was cleared in WT cells, the large inclusion persisted in over 50% of *rtn1 rtn2 yop1* cells, consistent with a delay in Ubc9ts degradation (Fig. 3f). Thus, the formation, dynamics and clearance of cytoplasmic Q-bodies rely on the integrity of a dynamic ER network (Fig. 3g).

The Hsp70-Hsp90 chaperone network mediates Q-body formation and clearance

The ATP-dependence of Q-body clearance resonates with previous data implicating the ATP-dependent Hsp70 and Hsp90 systems in misfolded protein QC (Table S1)[23-27]. Indeed, Hsp70, Hsp90 and the Hsp70 cofactor Hsp110/Sse1 are also required for degradation of misfolded Ubc9ts (Fig. 4b). At 37°C, the Hsp70 Ssa1 colocalized with all misfolded Ubc9ts Q-bodies (Fig. 4a). The role of Hsp70 in the Q-body pathway was examined using two Hsp70-deficient strains: *ssa1 ssa2*, lacking the two major SSA isoforms, and *ssa1ts ssa2 ssa3 ssa4*, containing a single temperature-sensitive SSA isoform and lacking the others[28]. Both strains yielded similar results (Fig. 4c and Fig. S3b). Even before the temperature shift, most cells contained a static bright cortical inclusion, indicating that Hsp70 contributes to conformational maintenance of Ubc9ts-GFP at the permissive temperature (Fig. 4c, video S6). After the shift, the number of puncta remained unchanged over 30 min: no coalescence of the faint additional puncta was detected and most of the misfolded protein was found in the large inclusion (Fig. 4c and d). Thus, Hsp70 is required for Q-body formation, maturation and clearance, consistent with biochemical experiments (Fig. 4b). Q-bodies still formed in Hsp90-deficient cells (*hsc82 hsp82ts*)[25], but their movement and coalescence were dramatically affected, associated with a strong defect in misfolded Ubc9ts-GFP degradation (Fig. 4b, e, f and video S7). Thus, Hsp90 also participates in Q-body dynamics and degradation, but acts after the initial formation of inclusions.

The activity of Hsp70 and its cooperation with Hsp90 is regulated by J-domain proteins (Fig. S3a). Since Ydj1 is ER-associated through a farnesyl group[29], we examined whether it helps to process ER-associated Q-bodies. *ydj1* cells contained more diffuse misfolded Ubc9ts than WT cells and numerous dim puncta at the periphery (Fig. 4g). Cells expressing the farnesylation defective mutant *ydj1*(C406S)[30] also displayed clusters of tiny cortical puncta that appeared unable to merge, suggesting a defect in Q-body coalescence (Fig. 4g and video S8). However, Ubc9ts was eventually degraded with similar kinetics as wild-type

(Fig. 4g, video S8 and Fig. S3c), perhaps due to the high level of redundancy between J-domain proteins[31]. Indeed, disruption of both Ydj1 and another ER-anchored J-domain protein, Hlj1, in the *hlj1 ydj1*-151 strain[32] strongly affected Q-body formation. Only faint Ubc9ts-GFP puncta were discernible in *hlj1 ydj1*-151 cells at 37°C (Fig. S3d). Thus, ER-anchored J-domain proteins, but perhaps also other homologues, participate in Q-body formation. The Hsp70 nucleotide exchange factor Sse1 also affected Q-body dynamics (Fig. 4h and video S6). *sse1* cells exhibited a significant delay in Q-body clearance, associated with Ubc9ts degradation impairment (Fig. 4b and Fig. S3e). We conclude that a chaperone network involving Hsp70, Hsp90 and their co-chaperones mediates the active formation and maturation of Q-bodies, as well as their degradation (Fig. 3i and Table S1).

Balance between addition and dissolution activities controls Q-body dynamics

We next examined the role of the disagregase Hsp104 and the small HSPs implicated in prion formation[33, 34] and aggregate management in proteasome-inhibited cells[6, 7, 14]. Live-cell imaging demonstrated that both Hsp104 and Hsp42 associate with Ubc9ts-CHFP Q-bodies formed upon heat stress (Fig. 5a-c; video S9). At 37°C, in absence of proteasome inhibition, Hsp104 and Hsp42 persist in the punctate Q-bodies structures even after Ubc9ts-CHFP degradation (Fig. 5a; video S9), suggesting that endogenous heat-denatured proteins are also concentrated and processed through the Q-body pathway. Accordingly, cells not expressing Ubc9ts, or expressing native Ubc9-GFP, also formed Hsp104-GFP and Hsp42-GFP containing puncta upon heat stress, which move and coalesce with similar dynamics as Ubc9ts Q-bodies (Fig. 5b; c). We conclude that Hsp42 and Hsp104 are components of endogenous Q-bodies, which form upon heat stress as a physiological response to misfolded proteins.

Interestingly, untreated and proteasome-inhibited cells exhibited differences in their Hsp104 and Hsp42 distribution. In untreated cells, Hsp42-GFP colocalized with all the Ubc9ts containing puncta (Fig. 5c), while in proteasome-inhibited cells, Hsp42 was absent from some inclusions[7]. Hsp104 did not co-localize with perinuclear puncta without proteasome inhibitor (Fig. 5b). The lack of Hsp104 in perinuclear puncta was confirmed by two-color Z-stack deconvolution and analysis of DAPI-labeled fixed cells (Fig. S4). Possibly, proteasome inhibition alters inclusion dynamics and composition, as inclusions continue coalescing and persist much longer in the cell.

We evaluated how Hsp104 and the small HSPs Hsp42 and Hsp26 participate in Q-body processing. In *hsp26* cells, the inclusion dynamics and Ubc9ts half-life were unaffected (Fig. 5d-f). In *hsp104* cells, misfolded Ubc9ts-GFP progressed from dim puncta to the formation of medium-intensity puncta, similar to WT cells. These medium-intensity puncta did not coalesce into few brighter inclusions as in WT cells, indicating that the progression of the pathway is blocked by loss of Hsp104 (Fig. 5d and e, video S10). In *hsp42*, only a handful of dim puncta formed after 10 min indicating a severe defect in Q-body formation (Fig. 5d, and video S10). Remarkably, Ubc9ts degradation was unaffected in both *hsp104* and *hsp42* strains (Fig. 5f). Thus, sequestration into larger inclusions is not essential for misfolded protein degradation.

The fact that puncta coalescence, but not degradation, requires a disaggregase such as Hsp104 is counter-intuitive; a simple model would predict that disaggregase deletion leads to formation of larger hard-to-degrade inclusions. We hypothesized that puncta coalescence may involve Hsp104-mediated dissolution of some puncta followed by re-addition of the released misfolded protein into existing inclusions (Fig. 5i). In this view, loss of puncta in *hsp42* cells would not reflect an absolute requirement of Hsp42 for Q-body formation but rather a shift in the balance between Hsp42-stimulated addition and Hsp104-stimulated dissolution. Indeed Ubc9ts inclusions were observed in the double *hsp42 hsp104* cells (Fig. 5g, video S10), indicating that Hsp42 is not required for inclusion formation. However, puncta intensity in *hsp42 hsp104* was heterogeneous and their coalescence was affected, consistent with Hsp104 promoting Q-body maturation into large inclusions. Notably, Ubc9ts degradation was unaffected in *hsp42 hsp104* cells (Fig. 5f). Hsp104 is not the only chaperone promoting Q-body dissolution, since the *hsp42 sse1* mutant also forms inclusions (Fig. 5h), albeit with severely affected dynamics. Thus, a chaperone-mediated balance between addition and dissolution regulates Q-body formation and maturation (Fig. 5i).

Soluble misfolded proteins, but not amyloidogenic IPOD substrates, transit through the Q-body pathway

The generality of the Q-body pathway was assessed by coexpressing Ubc9ts with two distinct QC substrates: misfolded variants of the tumor suppressor VHL or the thermolabile firefly luciferase (Luc)[25, 35]. These misfolded proteins also formed Q-bodies in distinguishable from those observed for Ubc9ts. The puncta formed by VHL or Luc completely colocalized with Ubc9ts Q-bodies, moved and coalesced together throughout the time-course of degradation (Fig. 6a, b; video S11, and Fig. S5a). Importantly, VHL did not colocalize non-specifically with wild-type Ubc9, which remains folded at 37°C (Fig. 6a). VHL puncta were generated regardless of the presence of Ubc9 and proceeded through the Q-body pathway (Fig. S5b). This indicates that different misfolded proteins are recruited to the same cellular structures and are handled by the same QC pathway.

We examined whether the Q-body pathway overlaps with insoluble amyloidogenic IPOD substrates such as the prion Rnq1 and the polyglutamine-expanded Huntingtin exon1 fragment, Htt-Q97 (Fig. 6e)[6]. Live-cell imaging of misfolded Ubc9ts or VHL in cells coexpressing either Htt-Q97 or Rnq1 indicated that most Ubc9ts or VHL puncta moved and evolved independently of the IPOD. A few dim puncta transiently colocalized with the IPOD, but without merging with it (Fig. 6c, d; video S11 and Fig. S5c). Notably, Q-body dynamics were slightly altered in the presence of Htt-Q97 or Rnq1, suggesting that the presence of amyloids in the IPOD can affect protein homeostasis. Ubc9ts and VHL were still cleared, while Rnq1 and Htt-Q97 persisted for the duration of the time-course (Fig. 6c, d; video S11 and Fig. S5c). These results reveal two major fates for misfolded proteins in the absence of proteasome inhibition.

Distinct role of chaperones in Q-body and IPOD formation

The different mechanisms to cope with misfolded proteins could stem from their distinct interactions with the chaperone machinery. Indeed, chaperones participate differently in Q-

body and IPOD formation, both qualitatively (Fig. 6f) and when quantifying the number of cells with inclusions over the population (Fig. 6g, h). Q-body substrates formed one major inclusion in *ssa1 ssa2* cells; large peripheral inclusions in *hsp104*, and no inclusions in *hsp42* cells. In contrast, IPOD substrates did not form any inclusions in *hsp104* mutant as described[36-38], and significantly less inclusions in *ssa1 ssa2* cells (Fig. 6f, h). Unlike Q-bodies, IPOD inclusions were still formed in *hsp42* mutant, even though they appeared dimmer (Fig. 6f). Hsp42 did not colocalize with the IPOD substrates in non-stressed cells, and weakly at higher temperatures (Fig. S5d and e), consistent with it being dispensable for IPOD formation. This may reflect the higher tendency of amyloidogenic proteins to self-assemble. Alternatively, IPOD substrates may be less dependent on the action of Hsp42 because they are more refractory to the disaggregase activity of Hsp104 and other chaperones.

Q-bodies arise in response to proteotoxic stress

We next examined whether Q-bodies arise generally upon proteotoxic stress. Cells were exposed to ethanol, which denatures pre-existing proteins[39], or treated with the proline analog azetidine 2-carboxylic acid (AZC), which causes misfolding upon incorporation into newly synthetized proteins[40]. Exposure at 37°C served as a positive control (Fig. 7a). Ubc9ts-GFP and Hsp104-GFP were used to visualize Q-bodies. Ethanol treatment was sufficient to generate Hsp104-GFP and Ubc9ts-GFP positive Q-bodies similar to those observed during heat stress (Fig. 7a). While their kinetics of appearance was faster during heat stress, Q-body dynamics and coalescence appeared similar in all treatments (Fig. 7a).

We determined whether generating newly synthesized misfolded proteins affects the state of pre-existing folded proteins. Synthesis of Ubc9ts was repressed by glucose addition at 28°C yielding a pool of pre-existing folded and diffusely localized Ubc9ts, which served as a sensor of general proteostasis in the cell. Newly translated misfolded proteins were generated by AZC treatment at 28°C. Strikingly, the pre-existing folded Ubc9ts-GFP re-localized to Q-bodies at 28°C after AZC addition, even though no new Ubc9ts protein was being translated (Fig. 7a). These results indicate that misfolding of newly made proteins shifts the proteostasis balance of the cell to induced misfolding of a pre-existing labile protein, likely because its folding depends on the continued action of chaperones.

The Q-body pathway is regulated by cellular status

Protein homeostasis is regulated by cellular status and is impaired during aging, which may account for the late-onset of many amyloid diseases[41-43]. We examined whether cellular state or aging modulate the formation and processing of Q-bodies. Budding yeast enter a non-diving G0-like state when a culture is grown to stationary phase, a paradigm often referred to as chronological aging[44]. Aged non-dividing cells expressing diffuse Ubc9ts-GFP were shifted to 37°C and imaged. None of the aged cells was capable of inducing Q-bodies, unlike what is observed in young dividing cells (Fig. 7b and Fig. S6). However, we did observe that aged cells contained pre-existing Hsp104-positive puncta as well as a distinct large inclusion containing Hsp42 (Fig. 7b), previously reported as a hallmark of chronologically aged cells[45].

The Q-bodies pathway is also regulated by TOR signaling, known to modulate protein homeostasis in response to nutrient and cellular state[42, 46, 47]. Treatment with 0.2 μg/ml rapamycin immediately prior to a 37°C shift profoundly affected the Q-body pathway (Fig. 7c, d, and video S12) leading to rapid clearance of Q-bodies from the cytoplasm. Our data imply a regulatory role of TOR signaling in the Q-body pathway, and suggest that aged cells have lost their responsiveness to spatially sequester misfolded proteins.

Fitness advantage of chaperones providing spatial sequestration of misfolded proteins

Despite their role in Q-body formation and dissolution, Hsp42 and Hsp104 are dispensable both for misfolded protein degradation and growth at 37°C (Fig. S7). However, the existence of a general pathway for the active spatial sequestration of misfolded proteins argues for a potential benefit to the cells. We hypothesized that sequestration into Q-bodies may purge the cellular milieu from potentially deleterious misfolded species, thereby providing a fitness advantage to cells during stress. To test this, we carried out competition experiments comparing the relative fitness of WT cells and cells lacking either Hsp42, Hsp26 or Hsp104 under normal and heat stress conditions. Equal amounts of WT and mutant cells were mixed and grown together at 28°C or 37°C, with daily dilutions, for 5 days. At each dilution, the proportion of WT and mutant cells was examined by comparing the number of kanamycin-resistant (kanR) colony-forming units (CFU) [i.e. mutant cells] vs. kanamycin-sensitive CFUs [i.e. WT cells] (Fig. 8a). Deletion of Hsp26 provides neither a fitness cost nor a benefit at either temperature. The equal proportion of WT and *hsp26* cells was maintained throughout the 5 days of growth at either temperature (Fig. 8b), also indicating that kanR does not affect the fitness of mutant cells. Deletion of Hsp42 provided neither cost nor benefit at 28°C (Fig. 8c, left panel). However, at 37°C, deletion of Hsp42 was remarkably disadvantageous as WT cells out competed *hsp42* cells after 2 days (Fig. 8c, right panel). Thus, Hsp42 provides a strong fitness advantage for cells subjected to stress. A parallel analysis for cells lacking Hsp104 proved surprising. Deletion of Hsp104 also reduced the fitness advantage of cells grown at 37°C (Fig. 8d, right panel) suggesting that protein disaggregation is advantageous under conditions of stress. However, under normal growth conditions, i.e. 28°C, Hsp104 has a strong fitness cost, as *hsp104* cells were much fitter than WT cells (Fig. 8d, left panel). Since the major biochemical and cellular function of Hsp104 is to disaggregate misfolded and aggregated proteins, this suggests that a strong disaggregase activity is disadvantageous in the absence of stress-induced protein misfolding.

Discussion

Misfolded protein clearance mechanisms were proposed to be hierarchical, whereby misfolded proteins are first stabilized by chaperones for either refolding or degradation with sequestration into inclusions as a second line of defense when proteostasis fails. Our study calls for a revision of this concept. We find that misfolded protein sequestration is a physiological and early response to the presence of misfolded proteins. Degradation occurs concurrently with Q-body processing, implying that sequestration is not necessarily a consequence of degradation failure. Q-bodies form in response to many stresses but become observable in larger inclusions upon proteostasis collapse, because their clearance is

abrogated while their formation and coalescence continues. Compartmentalization into Q-bodies is not essential for degradation but may enhance cell fitness by sequestering potentially toxic misfolded species. Our findings provide a simple explanation to the genesis of large inclusions upon protein homeostasis dysfunction and UPS impairment that does not require invoking activation of special inclusion-formation mechanisms.

Misfolded protein concentration into Q-bodies is an active process that requires molecular chaperones. The Hsp70-Hsp90-Hsp110 system, which also participates in the degradation and refolding of misfolded proteins[48, 49], is central to the formation and dynamics of Q-bodies. These chaperones likely constitute the core of the cytoplasmic QC system. Q-bodies are associated with the ER, which may provide a basis for Q-body movement and coalescence through its tubular and dynamic network throughout the cytosol. ER-associated J-domain proteins, Ydj1 and Hlj1[29, 32], are important for Q-body concentration and maturation, consistent with their role recruiting Ssa1 to the ER membrane[32, 50]. However, their function is not essential, likely due to functional overlaps between J-domain proteins[31].

The small HSP Hsp42 and the disaggregase Hsp104 contribute to Q-body dynamics. Epistasis analyses of mutations in Hsp42, Hsp104 and Hsp110/Sse1 suggest that at least part of Q-body dynamics results from the balance between addition and dissolution activities. A simple model explaining our data is that puncta formation involves the action of different chaperones, notably Hsp42 and J-domain proteins, whereas Q-body growth occurs at the expense of Hsp104 or Hsp110/Sse1-mediated dissolution of others. Interestingly, a similar cycle of addition-dissolution is proposed to govern P-granule dynamics and the asymmetric partition of maternally inherited mRNAs[51]. However, coalescence may also involve direct merging of Q-bodies with the help of chaperones and additional factors.

Q-body formation, dynamics and clearance are independent of either actin or tubulin cytoskeleton, consistent with previous analysis of the dynamics of Hsp104-associated proteins aggregates[52] and in contrast to alternative proposals[7, 14]. Importantly, our finding that prolonged depolymerization of the actin cytoskeleton has deleterious effects on the Q-body pathway suggests an explanation to reconcile these discrepancies. Unassembled actin may bind to and titrate QC components, generally impairing cellular proteostasis. The cytoskeleton may also be required for asymmetric partitioning of inclusions, a question that is not addressed here. Future studies incorporating our findings should illuminate the link between the cytoskeleton, protein homeostasis, and the inheritance of misfolded protein inclusions.

Without proteasome inhibition, misfolded proteins are not directly targeted to a static pre-existing QC compartment, but concentrated throughout the cell in multiple dynamic Q-bodies. The link between Q-bodies and compartments previously observed in presence of proteasome inhibition[6-8, 14] remains to be determined. These structures may be endpoints of the Q-body pathway resulting from the coalescence of Q-bodies when clearance is impaired. The observation that some perinuclear puncta lack Hsp104 can explain the appearance of the JUNQ upon proteasome inhibition; puncta with slower dissolution rates would eventually grow at the expense of those with higher Hsp104 levels and faster disaggregation kinetics. It

will be interesting to determine whether proteasome inhibition alters the composition and properties of these structures, for instance by stabilizing labile QC factors as suggested in [8].

Amyloidogenic proteins sequestered in the insoluble IPOD seem to bypass the Q-body pathway. Perhaps IPOD substrates interact aberrantly with chaperones that recruit substrates to the Q-body pathway thereby failing to be cleared. Alternatively, dense amyloid structures may be more refractory to disaggregation, thereby eluding the Q-body cycle. Interestingly, Q-body dynamics are impaired in presence of an IPOD suggesting that the IPOD alters cellular proteostasis. Several studies reported that amyloid inclusions sequester chaperones, causing aggregation of unrelated proteins without their co-aggregation with the amyloid inclusion[53, 54]. The impairment of the Q-body pathway during aging could render aged cells more sensitive to stress and misfolding, consistent with their enhanced sensitivity to protein misfolding[55]. Understanding the regulation of the Q-body pathway and its relation to other reported QC structures may provide new therapeutical targets for conformational disorders, including Alzheimer's and Huntington's disease.

What is the function of Q-bodies? Sequestering misfolded proteins is dispensable for degradation but may help clear the cytosol of potentially toxic misfolded species, store labile proteins for later use and/or facilitate QC by concentrating chaperones and substrates on a two-dimensional surface. Loss of chaperones involved in Q-body formation and dynamics leads to a fitness reduction in stressed cells. Surprisingly, the robust disaggregase Hsp104 is deleterious under normal growth conditions. This could explain the long-standing enigma of why Hsp104 is only found in yeast, plants and bacteria, generally subjected to repeated and severe stress[56], but not in metazoan cells, which control their stress responses through organism-wide cell non-autonomous circuits[57, 58]. For these multicellular organisms, the advantage provided by Hsp104 during stress may not compensate for the disadvantage of having a potent cellular disaggregase under normal conditions. These results highlight the delicate tuning of QC pathways during evolution.

Concentration of misfolded proteins in Q-bodies creates a dynamic and flexible management system conferring fitness pending the impact of the immediate environmental changes challenging the cell. The relationship between the biochemical functions of chaperones and their spatial organization within the cell will be instrumental to understand folding impairments during pathological states.

Supplementary Material

Refer to Web version on PubMed Central for supplementary material.

Acknowledgments

References

1. Balch WE, Morimoto RI, Dillin A, Kelly JW. Adapting proteostasis for disease intervention. Science. 2008; 319:916–919. [PubMed: 18276881]

2. Lindquist SL, Kelly JW. Chemical and biological approaches for adapting proteostasis to ameliorate protein misfolding and aggregation diseases: progress and prognosis. Cold Spring Harb Perspect Biol. 2011; 3

3. Chiti F, Dobson CM. Protein misfolding, functional amyloid, and human disease. Annual Review of Biochemistry. 2006; 75:333–366.

4. Houck SA, Singh S, Cyr DM. Cellular responses to misfolded proteins and protein aggregates. Methods Mol Biol. 2012; 832:455–461. [PubMed: 22350905]

5. Chen B, Retzlaff M, Roos T, Frydman J. Cellular strategies of protein quality control. Cold Spring Harb Perspect Biol. 2011; 3:a004374. [PubMed: 21746797]

6. Kaganovich D, Kopito R, Frydman J. Misfolded proteins partition between two distinct quality control compartments. Nature. 2008; 454:1088–1095. [PubMed: 18756251]

7. Specht S, Miller SB, Mogk A, Bukau B. Hsp42 is required for sequestration of protein aggregates into deposition sites in Saccharomyces cerevisiae. J Cell Biol. 2011; 195:617–629. [PubMed: 22065637]

8. Malinovska L, Kroschwald S, Munder MC, Richter D, Alberti S. Molecular chaperones and stress-inducible protein-sorting factors coordinate the spatiotemporal distribution of protein aggregates. Mol Biol Cell. 2012; 23:3041–3056. [PubMed: 22718905]

9. Johnston JA, Ward CL, Kopito RR. Aggresomes: a cellular response to misfolded proteins. J Cell Biol. 1998; 143:1883–1898. [PubMed: 9864362]

10. Zhang X, Qian SB. Chaperone-mediated hierarchical control in targeting misfolded proteins to aggresomes. Mol Biol Cell. 2011; 22:3277–3288. [PubMed: 21775628]

11. Douglas PM, Summers DW, Cyr DM. Molecular chaperones antagonize proteotoxicity by differentially modulating protein aggregation pathways. Prion. 2009; 3:51–58. [PubMed: 19421006]

12. Cohen E, Bieschke J, Perciavalle RM, Kelly JW, Dillin A. Opposing activities protect against age-onset proteotoxicity. Science. 2006; 313:1604–1610. [PubMed: 16902091]

13. Arrasate M, Mitra S, Schweitzer ES, Segal MR, Finkbeiner S. Inclusion body formation reduces levels of mutant huntingtin the risk of neuronal death. Nature. 2004; 431:805–810. [PubMed: 15483602]

14. Liu B, et al. The polarisome is required for segregation and retrograde transport of protein aggregates. Cell. 2010; 140:257–267. [PubMed: 20141839]

15. Nakatogawa H, Ichimura Y, Ohsumi Y. Atg8, a ubiquitin-like protein required for autophagosome formation, mediates membrane tethering and hemifusion. Cell. 2007; 130:165–178. [PubMed: 17632063]

16. Sheth U, Parker R. Targeting of aberrant mRNAs to cytoplasmic processing bodies. Cell. 2006; 125:1095–1109. [PubMed: 16777600]

17. Toshima JY, et al. Spatial dynamics of receptor-mediated endocytic trafficking in budding yeast revealed by using fluorescent alpha-factor derivatives. Proc Natl Acad Sci U S A. 2006; 103:5793–5798. [PubMed: 16574772]

18. Wright R, Basson M, D'Ari L, Rine J. Increased amounts of HMG-CoA reductase induce "karmellae": a proliferation of stacked membrane pairs surrounding the yeast nucleus. J Cell Biol. 1988; 107:101–114. [PubMed: 3292536]

19. Shibata Y, Voeltz GK, Rapoport TA. Rough sheets and smooth tubules. Cell. 2006; 126:435–439. [PubMed: 16901774]

20. Voeltz GK, Prinz WA, Shibata Y, Rist JM, Rapoport TA. A class of membrane proteins shaping the tubular endoplasmic reticulum. Cell. 2006; 124:573–586. [PubMed: 16469703]

21. Shibata Y, et al. The reticulon and DP1/Yop1p proteins form immobile oligomers in the tubular endoplasmic reticulum. J Biol Chem. 2008; 283:18892–18904. [PubMed: 18442980]

22. West M, Zurek N, Hoenger A, Voeltz GK. A 3D analysis of yeast ER structure reveals how ER domains are organized by membrane curvature. J Cell Biol. 2011; 193:333–346. [PubMed: 21502358]

23. McDonough H, Patterson C. CHIP: a link between the chaperone and proteasome systems. Cell Stress Chaperones. 2003; 8:303–308. [PubMed: 15115282]

24. Mayer MP, Bukau B. Hsp70 chaperones: cellular functions and molecular mechanism. Cell Mol Life Sci. 2005; 62:670–684. [PubMed: 15770419]

25. McClellan AJ, Scott MD, Frydman J. Folding and quality control of the VHL tumor suppressor proceed through distinct chaperone pathways. Cell. 2005; 121:739–748. [PubMed: 15935760]

26. Coppinger JA, et al. A chaperone trap contributes to the onset of cystic fibrosis. PLoS One. 2012; 7:e37682. [PubMed: 22701530]

27. Schneider C, et al. Pharmacologic shifting of a balance between protein refolding and degradation mediated by Hsp90. Proc Natl Acad Sci U S A. 1996; 93:14536–14541. [PubMed: 8962087]

28. Becker J, Walter W, Yan W, Craig EA. Functional interaction of cytosolic hsp70 and a DnaJ-related protein, Ydj1p, in protein translocation in vivo. Mol Cell Biol. 1996; 16:4378–4386. [PubMed: 8754838]

29. Caplan AJ, Tsai J, Casey PJ, Douglas MG. Farnesylation of YDJ1p is required for function at elevated growth temperatures in Saccharomyces cerevisiae. J Biol Chem. 1992; 267:18890–18895. [PubMed: 1527016]

30. Flom GA, Lemieszek M, Fortunato EA, Johnson JL. Farnesylation of Ydj1 is required for in vivo interaction with Hsp90 client proteins. Mol Biol Cell. 2008; 19:5249–5258. [PubMed: 18829866]

31. Kampinga HH, Craig EA. The HSP70 chaperone machinery: J proteins as drivers of functional specificity. Nat Rev Mol Cell Biol. 2010; 11:579–592. [PubMed: 20651708]

32. Youker RT, Walsh P, Beilharz T, Lithgow T, Brodsky JL. Distinct roles for the Hsp40 and Hsp90 molecular chaperones during cystic fibrosis transmembrane conductance regulator degradation in yeast. Mol Biol Cell. 2004; 15:4787–4797. [PubMed: 15342786]

33. Shorter J, Lindquist S. Hsp104, Hsp70 and Hsp40 interplay regulates formation, growth and elimination of Sup35 prions. EMBO J. 2008; 27:2712–2724. [PubMed: 18833196]

34. Tipton KA, Verges KJ, Weissman JS. In vivo monitoring of the prion replication cycle reveals a critical role for Sis1 in delivering substrates to Hsp104. Mol Cell. 2008; 32:584–591. [PubMed: 19026788]

35. Gupta R, et al. Firefly luciferase mutants as sensors of proteome stress. Nat Methods. 2011; 8:879–884. [PubMed: 21892152]

36. Chernoff YO, Lindquist SL, Ono B, Inge-Vechtomov SG, Liebman SW. Role of the chaperone protein Hsp104 in propagation of the yeast prion-like factor [psi+]. Science. 1995; 268:880–884. [PubMed: 7754373]

37. Sondheimer N, Lindquist S. Rnq1: an epigenetic modifier of protein function in yeast. Mol Cell. 2000; 5:163–172. [PubMed: 10678178]

38. Meriin AB, et al. Huntington toxicity in yeast model depends on polyglutamine aggregation mediated by a prion-like protein Rnq1. J Cell Biol. 2002; 157:997–1004. [PubMed: 12058016]

39. Piper PW. The heat shock and ethanol stress responses of yeast exhibit extensive similarity and functional overlap. FEMS Microbiol Lett. 1995; 134:121–127. [PubMed: 8586257]

40. Trotter EW, et al. Misfolded proteins are competent to mediate a subset of the responses to heat shock in Saccharomyces cerevisiae. J Biol Chem. 2002; 277:44817–44825. [PubMed: 12239211]

41. Morimoto RI. Proteotoxic stress and inducible chaperone networks in neurodegenerative disease and aging. Genes Dev. 2008; 22:1427–1438. [PubMed: 18519635]

42. Conn CS, Qian SB. mTOR signaling in protein homeostasis: less is more? Cell Cycle. 2011; 10:1940–1947. [PubMed: 21555915]

43. Taylor RC, Dillin A. Aging as an event of proteostasis collapse. Cold Spring Harb Perspect Biol. 2011; 3

44. Fabrizio P, Longo VD. The chronological life span of Saccharomyces cerevisiae. Aging Cell. 2003; 2:73–81. [PubMed: 12882320]

45. Narayanaswamy R, et al. Widespread reorganization of metabolic enzymes into reversible assemblies upon nutrient starvation. Proc Natl Acad Sci U S A. 2009; 106:10147–10152. [PubMed: 19502427]

46. Peters TW, et al. Tor1 regulates protein solubility in Saccharomyces cerevisiae. Mol Biol Cell. 2012; 23:4679–4688. [PubMed: 23097491]

47. Kapahi P, et al. With TOR, less is more: a key role for the conserved nutrient-sensing TOR pathway in aging. Cell Metab. 2010; 11:453–465. [PubMed: 20519118]

48. Glover JR, Lindquist S. Hsp104, Hsp70, and Hsp40: a novel chaperone system that rescues previously aggregated proteins. Cell. 1998; 94:73–82. [PubMed: 9674429]

49. Mandal AK, et al. Hsp110 chaperones control client fate determination in the hsp70-Hsp90 chaperone system. Mol Biol Cell. 2010; 21:1439–1448. [PubMed: 20237159]

50. Huyer G, et al. Distinct machinery is required in Saccharomyces cerevisiae for the endoplasmic reticulum-associated degradation of a multispanning membrane protein and a soluble luminal protein. J Biol Chem. 2004; 279:38369–38378. [PubMed: 15252059]

51. Ouellet J, Barral Y. Organelle segregation during mitosis: Lessons from asymmetrically dividing cells. J Cell Biol. 2012; 196:305–313. [PubMed: 22312002]

52. Zhou C, et al. Motility and segregation of Hsp104-associated protein aggregates in budding yeast. Cell. 2011; 147:1186–1196. [PubMed: 22118470]

53. Gidalevitz T, Krupinski T, Garcia S, Morimoto RI. Destabilizing protein polymorphisms in the genetic background direct phenotypic expression of mutant SOD1 toxicity. PLoS Genet. 2009; 5:e1000399. [PubMed: 19266020]

54. Olzscha H, et al. Amyloid-like aggregates sequester numerous metastable proteins with essential cellular functions. Cell. 2011; 144:67–78. [PubMed: 21215370]

55. Kikis EA, Gidalevitz T, Morimoto RI. Protein homeostasis in models of aging and age-related conformational disease. Adv Exp Med Biol. 2010; 694:138–159. [PubMed: 20886762]

56. Shorter J. Hsp104: a weapon to combat diverse neurodegenerative disorders. Neurosignals. 2008; 16:63–74. [PubMed: 18097161]

57. Gidalevitz T, Prahlad V, Morimoto RI. The stress of protein misfolding: from single cells to multicellular organisms. Cold Spring Harb Perspect Biol. 2011; 3

58. Durieux J, Wolff S, Dillin A. The cell-non-autonomous nature of electron transport chain-mediated longevity. Cell. 2011; 144:79–91. [PubMed: 21215371]
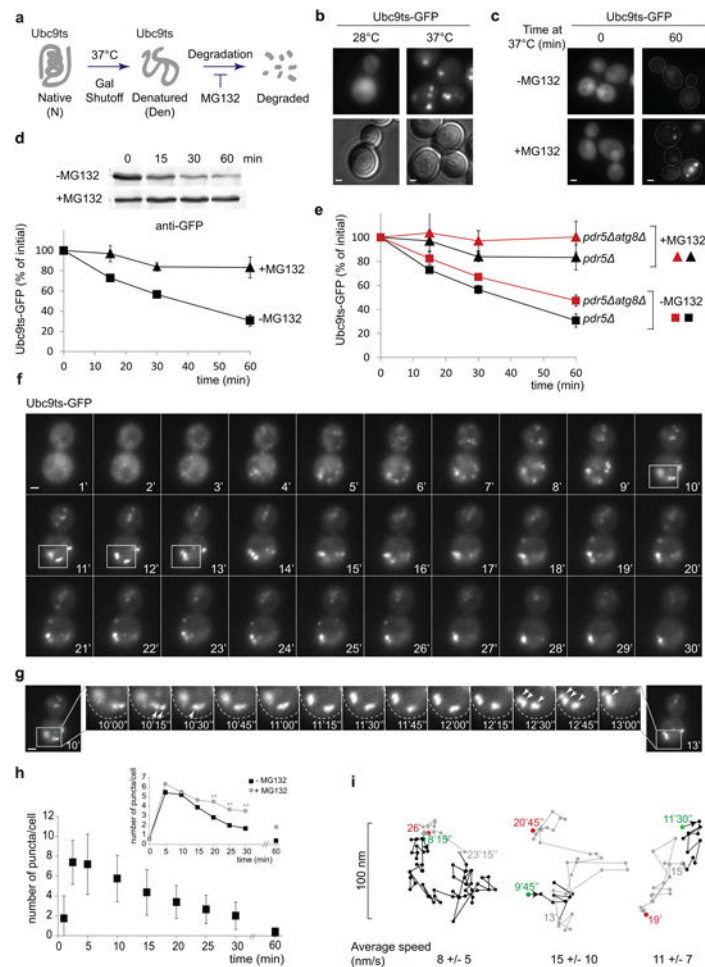
Figure 1. Misfolded proteins are sequestered in Q-bodies upon heat stress

(**a**) Ubc9ts-GFP fate upon heat stress. (**b**) Ubc9ts-GFP expressed in WT cells at 28°C was shifted for 15 min at 37°C. GFP (upper panel) and DIC (lower panel) are shown. Scale bars equal 1.5 μm. (**c**) *pdr5* cells expressing Ubc9ts-GFP were grown at 28°C in galactose medium and shifted to 37°C in glucose medium with (+) or without (-) 100 μM MG132. Images show Ubc9ts-GFP at the shift (t=0) and after 60 min (t=60). Dotted lines highlight cell outlines. Scale bar equals 1μm. (**d**) As in **c**, Ubc9ts-GFP was immunoblotted with anti-GFP antibodies and quantified as the relative ratio to the initial amount for each condition. Results represent mean and Standard Deviation (SD) of three independent experiments. (**e**) *pdr5* and *pdr5 atg8* cells expressing Ubc9ts-GFP were grown as in **c**. Ubc9ts-GFP was immunoblotted with anti-GFP antibodies (Fig. S1b) and quantified relative to the initial amount for each condition. Results represent mean and SD of three independent experiments. (**f**) WT cells expressing Ubc9ts-GFP at 28°C in galactose medium were shifted at 37°C in glucose medium. Time series images show GFP signal in a cell 1 min (1′) to 30 min (30′) after the shift (video S1). Scale bar equals 1 μm. (**g**) Inset in **f**, highlights the coalescence of Ubc9ts-GFP Q-bodies (arrows), from 10 to 13 min after the shift. (**h**) Number of puncta in the medial focal plane over time in WT (main panel; puncta assessed from a total population of n=63 cells over three independent experiments, 1 field counted

per experiment) or in *pdr5* cells (puncta assessed from a total population of n=36 cells over three independent experiments, 1 field counted per experiment) with or without MG132 (secondary panel). Results represent mean of puncta for n cells and SD. (**) p<0.005, compared to untreated cells for the same indicated time. (**i**) Trajectories of three Ubc9-GFP Q-bodies in WT cells. Positions of particles are represented from each frame of a movie (1 frame/15 sec) at the medial focal plane. Consecutive positions are connected by lines: black, before coalescence; grey, after coalescence. Green and red dots indicate the initial and final positions, respectively. Initial, final and coalescing times are indicated, and average speed (+/- SD) over the entire trajectory.
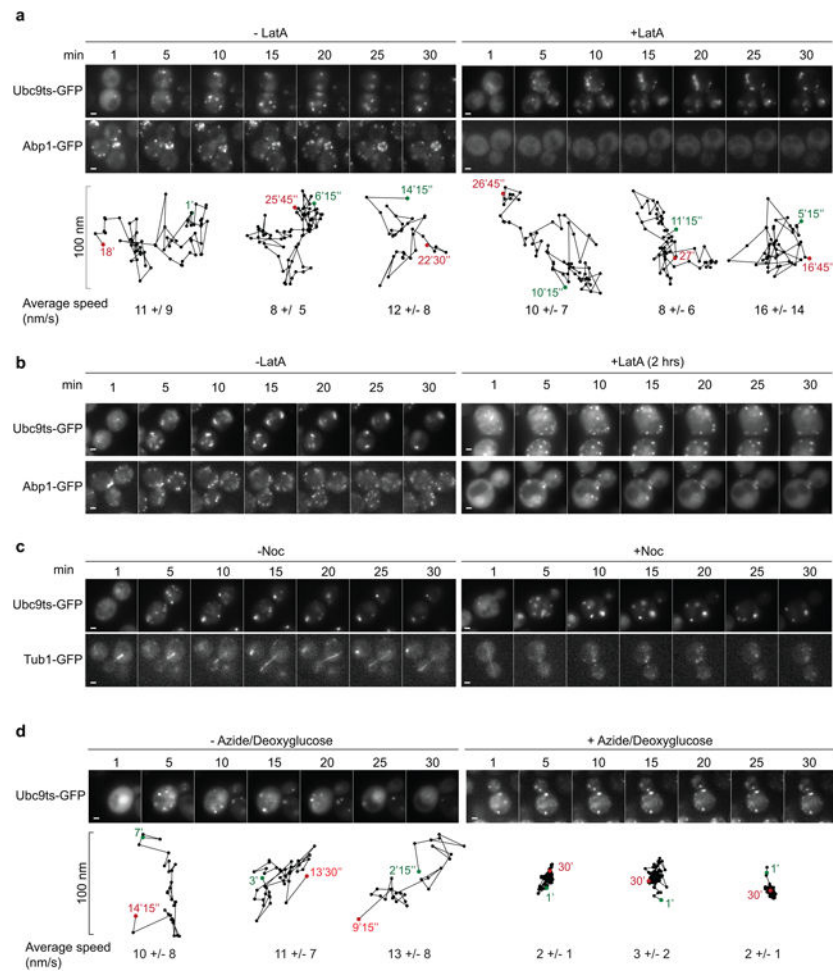
Figure 2. Energy dependence but cytoskeleton independence of Q-body dynamics
(**a**) WT cells expressing Ubc9ts-GFP or Abp1-GFP (lower panel) were grown at 28°C in galactose medium and treated with (right panel) or without (left panel) 200 μM Latrunculin A (LatA) for 10 min prior to a shift to 37°C in glucose medium. 5 min series of images show Ubc9ts-GFP or Abp1-GFP signal (video S2). Scale bars equal 1 μm. Trajectories of three Ubc9-GFP puncta in WT cells with or without LatA are represented (lower panel) as described in Fig. 1i. (**b**) WT cells expressing Ubc9ts-GFP and Abp1-GFP were grown as in **a** but treated with (right panel) or without (left panel) LatA for 2h prior to the shift. Scale bars equal 1 μm. (**c**) WT cells expressing Ubc9ts-GFP or Tub1-GFP were grown as in **a** but treated with (lower panel) or without (upper panel) 15 μg/ml Nocodazole (Noc) for 10 min prior to the shift. 5 min series of images show Ubc9ts-GFP or Tub1-GFP signal. Scale bars equal 1 μm. (**d**) WT cells expressing Ubc9ts-GFP were grown as in **a** but treated for 30 min with (right panel) or without (left panel) 10 mM azide and deoxyglucose prior to the shift. 5 min series of images show Ubc9ts-GFP signal (video S3). Scale bars equal 1 μm. Trajectories of three Ubc9-GFP puncta in cells with and without azide and deoxyglucose treatment are represented (lower panel) as described in Fig. 1i.
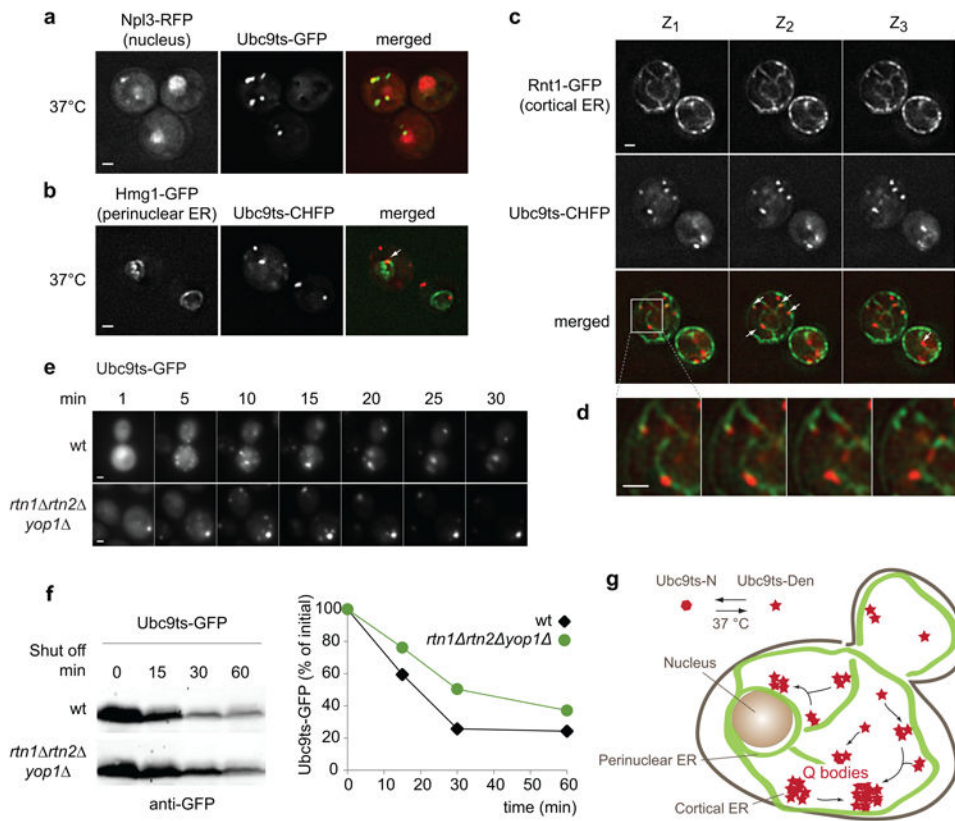
Figure 3. Q-body dynamics relies on an intact cortical ER
(**a**) Cells expressing Npl3-RFP and Ubc9ts-GFP were imaged after 10 min at 37°C. Two-color deconvolved images show Npl3-RFP signal (nucleus) in red and Ubc9ts-GFP signal in green. Scale bar equals 1 μm. (**b**) Cells expressing Hmg1-GFP (perinuclear ER, green) and Ubc9ts-CHFP (red) were imaged as in **a**. Arrow indicates Q-body in proximity to the ER. Scale bar equals 1 μm. (**c**) Cells expressing Rtn1-GFP and Ubc9ts-CHFP were imaged after 10 min at 37°C. Two-color images of three Z-focal plans (0.2 μm intervals) show Rtn1-GFP signal (cortical ER) in green and Ubc9ts-CHFP signal in red (video S4). Arrows indicate Q-bodies in proximity to the cortical ER. Scale bar equals1 μm. (**d**) Inset from **c** representing a series of 0.2 μm Z-section. Scale bar equals 1 μm. (**e**) Ubc9ts-GFP was expressed in WT and *rnt1 rtn2 yop1* cells at 28°C in galactose medium and shifted at 37°C in glucose medium. 5 min series of images show Ubc9ts-GFP signal over 30 min. Scale bars equal 1 μm. (**f**) As in **e**, cells were harvested at indicated time from the shift and Ubc9ts-GFP was immunoblotted with anti-GFP antibodies. Ubc9ts-GFP was quantified as the relative ratio to the initial amount from one experiment representative of four independent experiments. (**g**) Schematic of ER-associated Q-body processing of misfolded Ubc9ts (red star). Green represents the ER network throughout the cell.
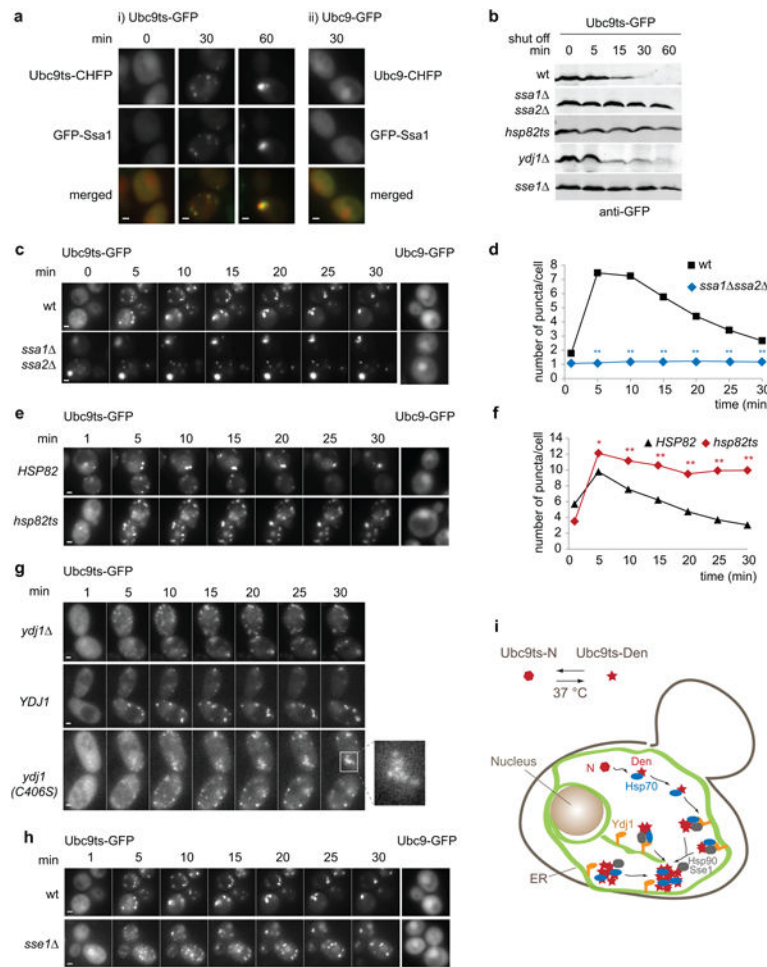
Figure 4. The maturation and degradation of Q-bodies rely on the Hsp70-Hsp90 system
(**a**) WT cells co-expressing GFP-Ssa1 and Ubc9ts-CHFP, or GFP-Ssa1 and Ubc9-CHFP, were grown at 28°C in galactose medium and shifted to 37°C in glucose medium. Two-color images show GFP-Ssa1 signal in green and Ubc9ts-CHFP signal in red at 0, 30 and 60 min after the shift. Scale bars equal 1.5 μm. (**b**) Cells expressing Ubc9ts-GFP at 28°C in galactose medium were shifted at 37°C (t=0) in glucose medium. Cells were harvested at indicated times and Ubc9ts-GFP immunoblotted using anti-GFP antibodies. (**c**) Ubc9ts-GFP was expressed in WT and *ssa1 ssa2* cells at 28°C in galactose medium and shifted at 37°C in glucose medium. 5 min series of images show Ubc9ts-GFP signal over 30 min (i). Cells expressing Ubc9-GFP were similarly prepared and imaged 15 min after the shift (ii). Scale bars represent 1 μm. (**d**) Average number of puncta per cell in WT (black squares) and *ssa1 ssa2* (blue diamonds) cells over time. Puncta assessed from a total population of n=35 cells over three independent experiments (1 field counted per experiment).(**) p<0.005 compared to WT for the same indicated time. (**e**) WT and *hsp82ts* cells expressing Ubc9ts-GFP or Ubc9-GFP were prepared and imaged as in **c**. Scale bars represent 1 μm. (**f**) Average number of puncta per cell in WT (black triangles) and *hsp82ts* (red diamonds) cells over time. Puncta assessed from a total population of n=25 cells over two independent experiments (1 field counted per experiment).(*) p<0.05 (**) p<0.005 compared to WT for

the same indicated time. (**g**) *ydj1* strains expressing Ubc9ts-GFP alone, and in combination with *YDJ1*, *ydj1*(C406S) or empty vector was prepared and imaged as in **c**. Shown an inset of a *ydj1*(C406S)-expressing cell. Scale bars represent 1 μm. (**h**) WTor*sse1* cells expressing Ubc9ts-GFP or Ubc9-GFP were prepared and imaged as in **c**. Scale bars represent 1 μm. (**i**) Role of the Hsp70-Hsp90-Hsp110 system in Q-bodies pathway for misfolded Ubc9ts (red star). Green represents the ER network throughout the cell.
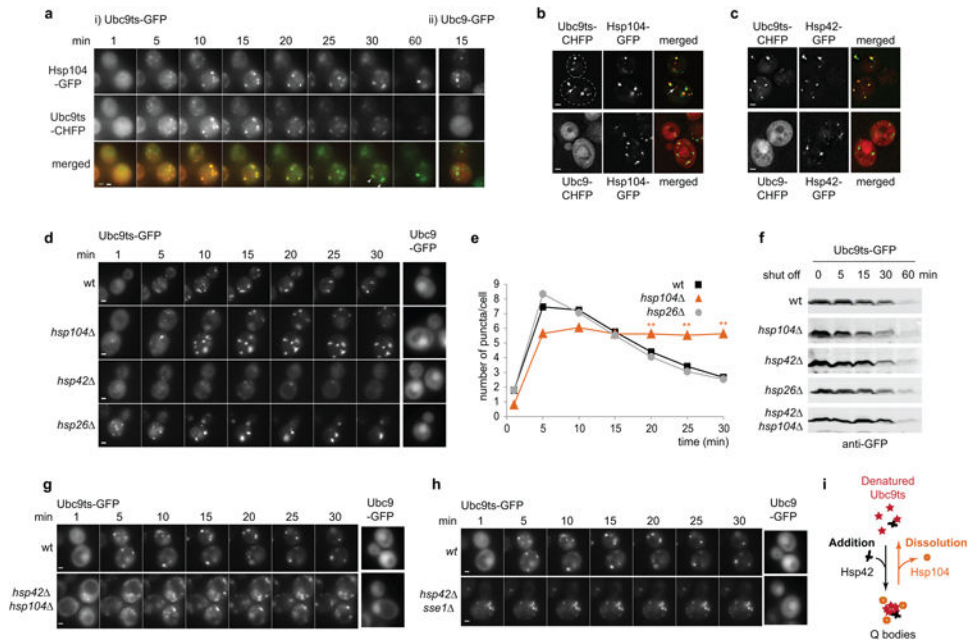
Figure 5. Balance between addition and dissolution activities controls Q-body dynamics
(**a**) Cells expressing Hsp104-GFP and Ubc9ts-CHFP or Ubc9-GFP were grown at 28°C in galactose medium and shifted at 37°C in glucose medium. 5 min series of a two-color movie show Hsp104-GFP signal in green and Ubc9ts-CHFP signal in red over 60 min (i). Cells expressing Hsp104-GFP and Ubc9-CHFP were imaged 15 min after the shift (ii). Scale bar equals 1 μm. (**b**) As in **a**, but cells were imaged 10 min after the shift. Two-color deconvolved images show Hsp104-GFP signal in green and Ubc9ts-CHFP or Ubc9-CHFP signal in red. Scale bars represent 1 μm. (**c**) Cells expressing Hsp42-GFP (green) and Ubc9ts-CHFP or Ubc9-CHFP (red) were imaged as in **b**. Scale bars equal 1 μm. (**d**) WT, *hsp104* , *hsp42* , and *hsp26* cells expressing Ubc9ts-GFP (i) or Ubc9-GFP (ii) were prepared as in **a**. 5 min series of images show Ubc9ts-GFP signal over 30 min. Ubc9-GFP signal is shown 15 min after the shift. Scale bars represent 1 μm. (**e**) Average number of puncta per cell in the WT (black squares), *hsp104* (orange diamonds), *hsp26* (gray circles) strains over time. Puncta assessed from a total population of n=35 cells over three independent experiment (1 field counted per experiment). (*) $p < 0.05$ (**) $p < 0.005$ compared to WT for the same indicated time. (**f**) Indicated strains expressing Ubc9ts-GFP were grown as in **a** and harvested at indicated times from the shift (t=0). Ubc9ts-GFP was immunoblotted using anti-GFP antibodies. (**g**) WT and *hsp42 hsp104* cells expressing Ubc9ts-GFP and Ubc9-GFP were prepared and imaged as in **d**. Scale bars represent 1 μm. (**h**) WT and the *hsp42 sse1* cells expressing Ubc9ts-GFP and Ubc9-GFP were prepared and imaged as in **d**. Scale bars represent 1 μm. (**i**) Dissolution-addition balance between Hsp104 and Hsp42: Q-body coalescence results from an Hsp104-mediated process of dissolution followed by Hsp42 stimulated re-addition of the released misfolded protein into existing inclusions.
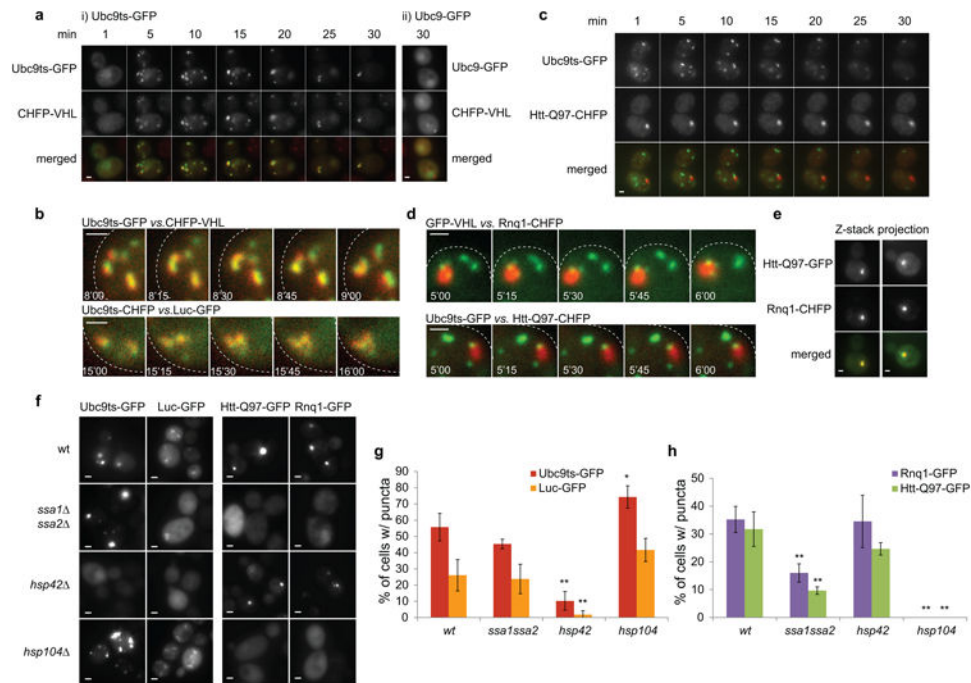
Figure 6. Different types of misfolded proteins, but not amyloids, are processed together through the Q-body pathway

(**a**) WT cells expressing Ubc9ts-GFP and CHFP-VHL was grown at 28°C in galactose medium and imaged at 37°C in glucose medium. 5 min series of images show Ubc9ts-GFP signal in green and CHFP-VHL signal in red (i). Cells expressing Ubc9-GFP and CHFP-VHL were similarly prepared and imaged 15 min after the shift (ii). Scale bar equals 1 μm. (**b**) 15 sec interval series of an inset from cell represented in **a** (top panel) and from a cell co-expressing Luc-GFP and Ubc9-CHFP (bottom panel, and Fig. S5a). Scale bars equal 1 μm (**c**). WT cells expressing Htt-Q97-CHFP (red) and Ubc9ts-GFP (green) were prepared and imaged as in **a**. Scale bar equals 1 μm. (**d**) 15 sec interval series of an inset from cell represented in **c** (bottom panel) and from a cell co-expressing GFP-VHL and Rnq1-CHFP (top panel, and Fig. S5c). Scale bars equal 1 μm. (**e**) Two-color Z-stack projection of cells expressing both Htt-Q97-GFP (in green) and Rnq1-CHFP (in red). Scale bar equals 1 μm. (**f**) GFP signal of WT, *ssa1 ssa2*, *hsp42*, *hsp104* cells expressing Ubc9ts-GFP or Luc-GFP at 37°C; or Htt-Q97-GFP or Rnq1-GFP at 28°C. Scale bars equal 1 μm.(**g-h**) Percentages of cells with puncta from a population analyzed in **f**. Respective total population sizes for WT, *ssa1ssa2*, *hsp42*, and *hsp104* cells are [(**g**): orange n=(2418, 375, 3013, 591) cells; yellow n=(1035, 472, 442, 681) cells; (**h**): purple, n=(971, 519, 1047, 617) cells; green n=(1165, 410, 1235, 853) cells] over three independent experiments.(6 fields counted per experiment) (*) $p<0.05$ (**) $p<0.005$ compared to WT for the same indicated time.
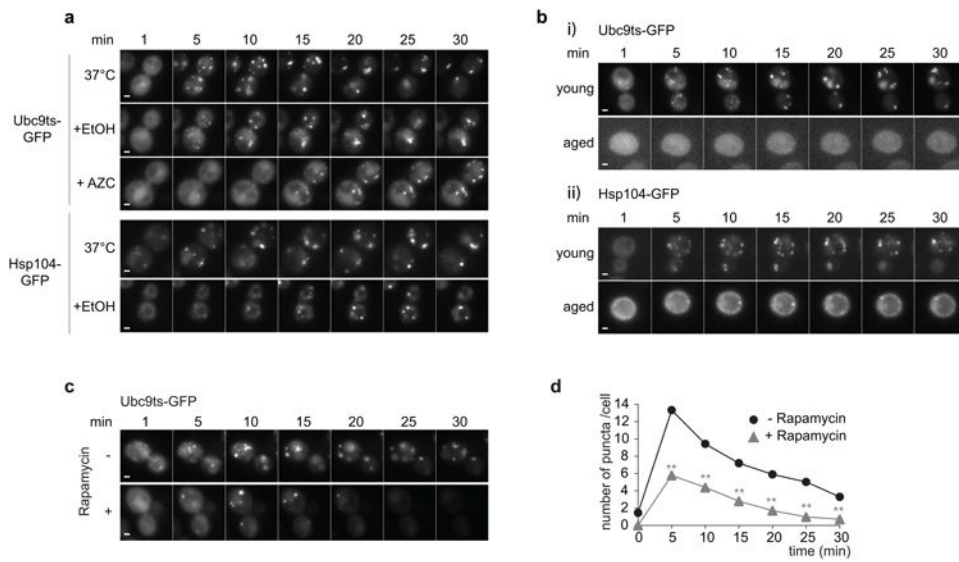
Figure 7. The Q-body pathway responds to proteotoxic stress, chronologic aging and nutrient signaling

(**a**) Ubc9ts-GFP-expressing cells were grown at 28°C in galactose medium and Hsp104-GFP-expressing at 28°C in glucose medium. Cells were imaged at 28°C in glucose medium after a 10 min treatment with 10% ethanol (EtOH), 30 min treatment with 5 mg/mL AZC, or at 37°C with no treatment. GFP signal is shown in 5 min series movies over 30 min. Scale bars equal 1 μm. (**b**) Cells expressing Ubc9ts-GFP (i) or Hsp104-GFP (ii) were grown at 28°C for 5 hrs (young) or for 3 days (aged) and imaged at 37°C. GFP signal is shown in 5 min series movies. Scale bars equal 1 μm. (**c**) Ubc9ts-GFP-expressing cells were grown at 28°C in galactose medium and imaged at 37°C in glucose medium in the absence (-) or presence (+) of 0.2 μg/mL rapamycin 10 min prior the shift. GFP signal is shown in 5 min series movies over 30 min. Scale bars equal 1 μm. (**d**) Quantification of the average number of puncta per cell in untreated (-, circles) or rapamycin-treated (+, triangles) cells over time as presented in **c**. Puncta assessed from a total population of n=40 cells over three independent experiment (3 fields counted per experiment).(*) $p < 0.05$ (**) $p < 0.005$ compared to untreated cells for the same indicated time.
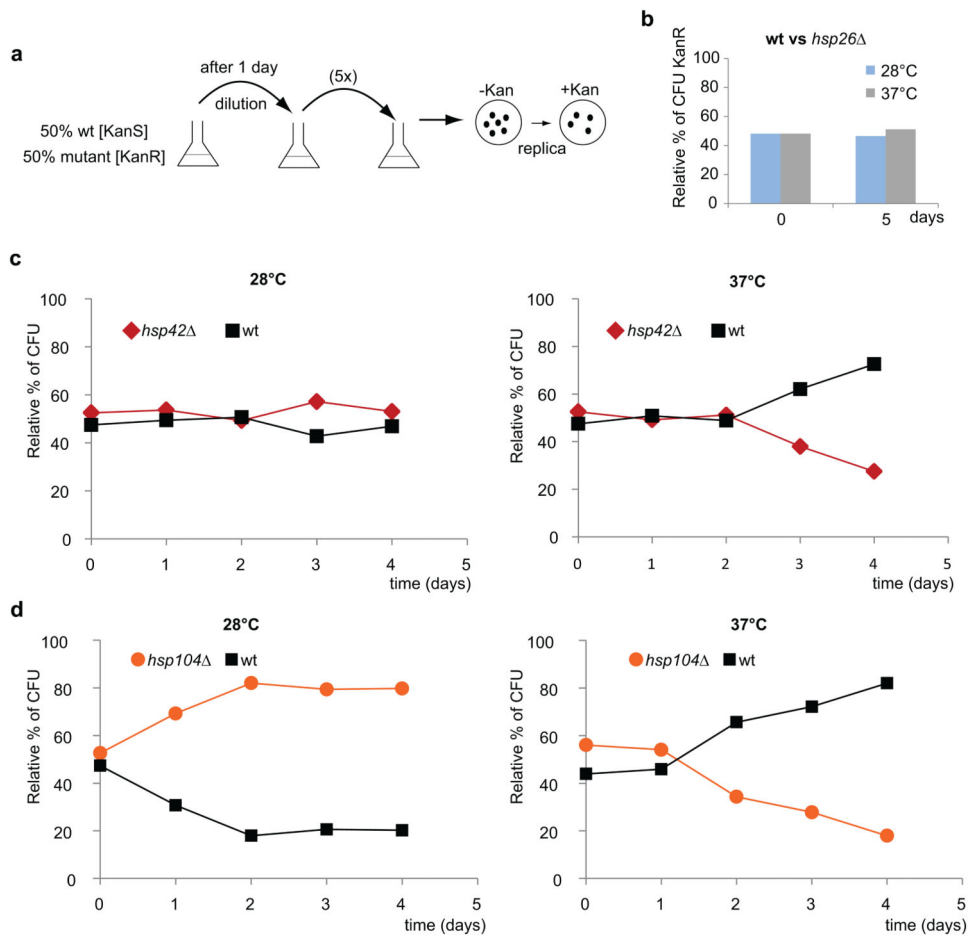
Figure 8. Fitness advantage of spatial sequestration of misfolded proteins in Q-bodies
(**a**) Schematic of competition assay; [KanS], kanamycin-sensitive phenotype; [KanR], kanamycin-resistant phenotype. (**b**) Percentage of KanR *hsp26* colony-forming units (CFU) over KanS WT CFU was quantified at 0 and 5 days. (**c-d**) Percentage of KanR *hsp42* CFU (**c**) or *hsp104* CFU (**d**) over KanS WT CFU was quantified over time at 28°C (left panels) or 37°C (right panels). Data represent three independent experiments (n = 350 CFU for each day of the experiment).